Sec. 4   Results

Question. Is the star formation model implemented for the Auriga simulations capable of producing a population of star particles that is consistent with the observed properties of the Milky Way (MW) globular cluster system (GCS)?

- What data do we have available for MW and M31?

- Does Auriga's star formation model produce sufficient star particles with the right age and metallicity ([Fe/H]) to be consistent with the MW GCS?

- Does Auriga's star formation model produce sufficient star particles with the right age and radial distribution to be consistent with the MW GCS?

- Does Auriga's star formation model produce sufficient star particles with the right age, metallicity ([Fe/H]) and radial distribution to be consistent with the MW GCS?

Question. What does the picture look like when broaden the scope to consider spirals in the Local Group (i.e. including Andromeda/M31)?

Assumption I. All star particles in the Auriga simulations with age > 10 Gyr are globular cluster candidates.

Justification

i) VandenBerg et al. (2013) measured [Fe/H] of 55 globular clusters in the MW and obtained age-estimates. The mean age of the MW GCS is 11.9 Gyr with a dispersion of 0.9 Gyr. Furthermore, only one of the 55 GC age-estimates is below 10 Gyr.

ii) Renaud et al. (2017) performed one simulation of a MW-like galaxy (down to z=0.5, $T_{lookback} \approx 5$ Gyr) and performs the entire analysis using a subset of star particles with ages > 10 Gyr that is referred to as 'globular cluster candidates'.

Weaknesses

i) Pfeffer et al. (2018) show that star clusters do not simply follow the same distribution as the field stars. In our approach we don't just oversample the 'real' population of globular clusters (by ignoring/excluding dynamical evolution), but the retrieved distributions of old star particles in the simulations may not even faithfully represent the 'true' distribution of globulars.

ii) Caldwell et al. (2011) measured [Fe/H] of 87 globular clusters in M31 and obtained age-estimates. The mean age is 10.8 Gyr with a dispersion of 2.3 Gyr. Furthermore, 27 GCs have age-estimates below 10 Gyr, with a minimum age-estimate of 4.8 Gyr. Perhaps an age cut of 6 Gyr would would be more appropriate for M31, see Fig. **??**.
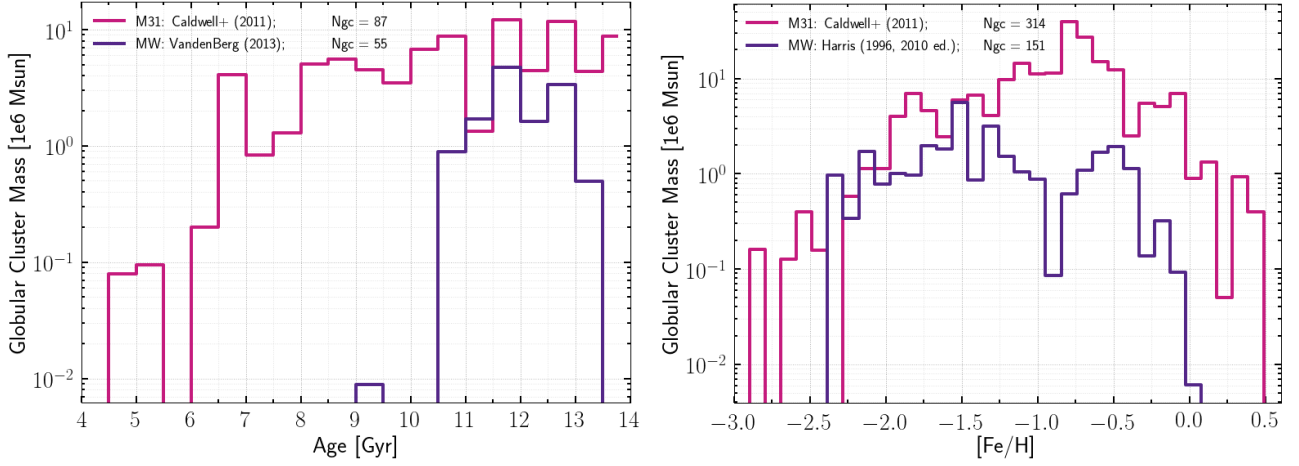
4.0 Available data for the Milky Way and Andromeda

Fig. 1: *Left:* Mass-weighted age distribution of 55 GCs in the MW (data from VandenBerg et al., 2013) and 87 GCs in M31 (data from Caldwell et al., 2011). *Right:* Mass-weighted [Fe/H] distribution of 151 GCs in the MW (data from Harris, 1996, 2010 ed.) and 314 GCs in M31.
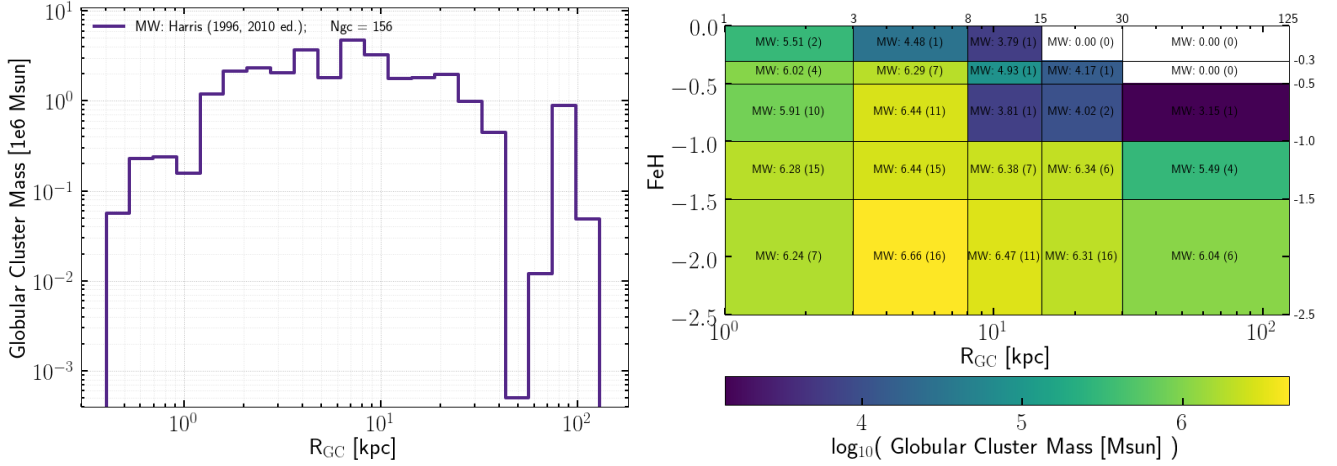

Fig. 2: *Left:* Mass-weighted r_{gc} distribution of 156 GCs in the MW. *Right:* Mass-weighted [Fe/H]-r_{gc} distribution of 151 GCs in the MW (data from Harris, 1996, 2010 ed.), which is 98.19 % of the total MW GCS mass.
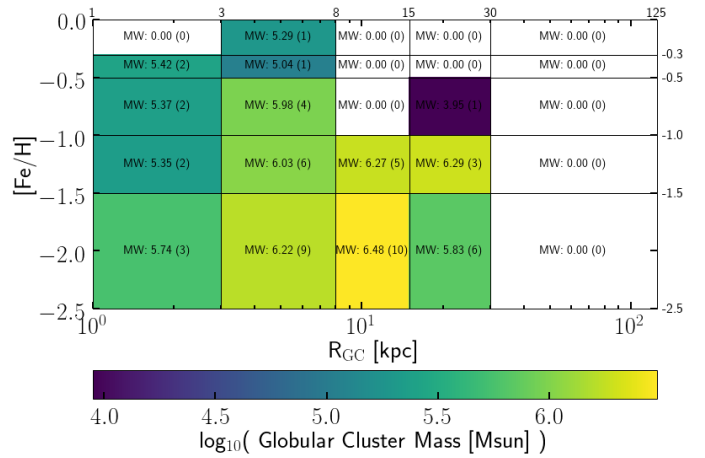

Fig. 3: Mass-weighted [Fe/H]-r_{gc} distribution of 55 GCs in the Milky Way (data from VandenBerg et al., 2013), which is 43.27% of the total MW GCS mass.

Table 1: The [Fe/H]-R_{GC} plot is generated using scipy.stats.binned_statistic_2d. This table shows a manual calculation of Msum and Ngc in each bin for debug purposes, just to check that scipy's built-in method is used correctly. Data from Harris (1996, 2010 ed.).

xmin	xmax	ymin	ymax	Ngc	Msum	$\log_{10}$(Msun)
1	3	-2.5	-1.5	7	1.7e+06	6.24
1	3	-1.5	-1.0	15	1.9e+06	6.28
1	3	-1.0	-0.5	10	8.2e+05	5.91
1	3	-0.5	-0.3	4	1.0e+06	6.02
1	3	-0.3	0	2	3.2e+05	5.51
3	8	-2.5	-1.5	16	4.6e+06	6.66
3	8	-1.5	-1.0	15	2.8e+06	6.44
3	8	-1.0	-0.5	11	2.8e+06	6.44
3	8	-0.5	-0.3	7	1.9e+06	6.29
3	8	-0.3	0	1	3.0e+04	4.48
8	15	-2.5	-1.5	11	3.0e+06	6.47
8	15	-1.5	-1.0	7	2.4e+06	6.38
8	15	-1.0	-0.5	1	6.5e+03	3.81
8	15	-0.5	-0.3	1	8.5e+04	4.93
8	15	-0.3	0	0	0.0e+00	-inf
15	30	-2.5	-1.5	16	2.1e+06	6.31
15	30	-1.5	-1.0	6	2.2e+06	6.34
15	30	-1.0	-0.5	2	1.0e+04	4.02
15	30	-0.5	-0.3	1	1.5e+04	4.17
15	30	-0.3	0	0	0.0e+00	-inf
30	125	-2.5	-1.5	6	1.1e+06	6.04
30	125	-1.5	-1.0	4	3.1e+05	5.49
30	125	-1.0	-0.5	1	1.4e+03	3.15
30	125	-0.5	-0.3	0	0.0e+00	-inf
30	125	-0.3	0	0	0.0e+00	-inf
Data from VandenBerg et al. (2013, 55 GCs)						
xmin	xmax	ymin	ymax	Ngc	Msum	$\log_{10}$(Msun)
1	3	-2.5	-1.5	3	5.5e+05	5.74
1	3	-1.5	-1.0	2	2.2e+05	5.35
1	3	-1.0	-0.5	2	2.3e+05	5.37
1	3	-0.5	-0.3	2	2.6e+05	5.42
1	3	-0.3	0	0	0.0e+00	-inf
3	8	-2.5	-1.5	9	1.7e+06	6.22
3	8	-1.5	-1.0	6	1.1e+06	6.03
3	8	-1.0	-0.5	4	9.6e+05	5.98
3	8	-0.5	-0.3	1	1.1e+05	5.04
3	8	-0.3	0	1	1.9e+05	5.29
8	15	-2.5	-1.5	10	3.0e+06	6.48
8	15	-1.5	-1.0	5	1.9e+06	6.27
8	15	-1.0	-0.5	0	0.0e+00	-inf
8	15	-0.5	-0.3	0	0.0e+00	-inf
8	15	-0.3	0	0	0.0e+00	-inf
15	30	-2.5	-1.5	6	6.8e+05	5.83
15	30	-1.5	-1.0	3	1.9e+06	6.29
15	30	-1.0	-0.5	1	8.9e+03	3.95
15	30	-0.5	-0.3	0	0.0e+00	-inf
15	30	-0.3	0	0	0.0e+00	-inf
30	125	-2.5	-1.5	0	0.0e+00	-inf
30	125	-1.5	-1.0	0	0.0e+00	-inf
30	125	-1.0	-0.5	0	0.0e+00	-inf
30	125	-0.5	-0.3	0	0.0e+00	-inf
30	125	-0.3	0	0	0.0e+00	-inf

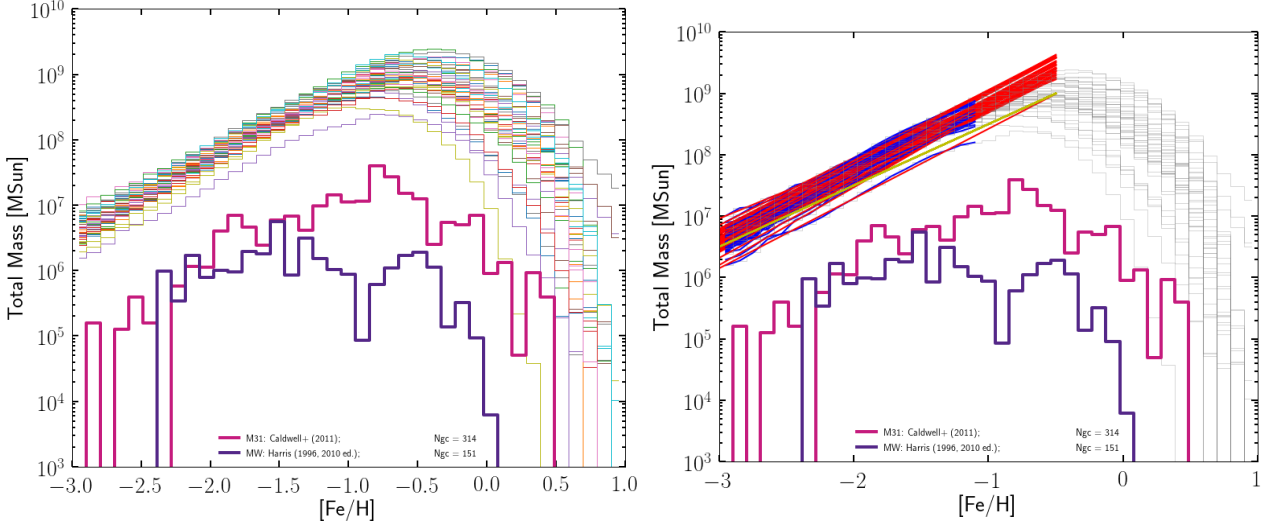# 4.1 Distribution of metallicity [Fe/H]

Fig. 4: *Left:* Mass-weighted [Fe/H] distribution of all Auriga haloes (level 3, 4 and 5). *Right:* There seems to be a trent of constant mass increase with increasing metallicity in the range -3 to -1, and roughly 1 order of magnitude scatter in mass normalization. We use linear regression to obtain $\log_{10}$(mass normalization) (i.e. we fit $a \cdot (x + 3) + b$)
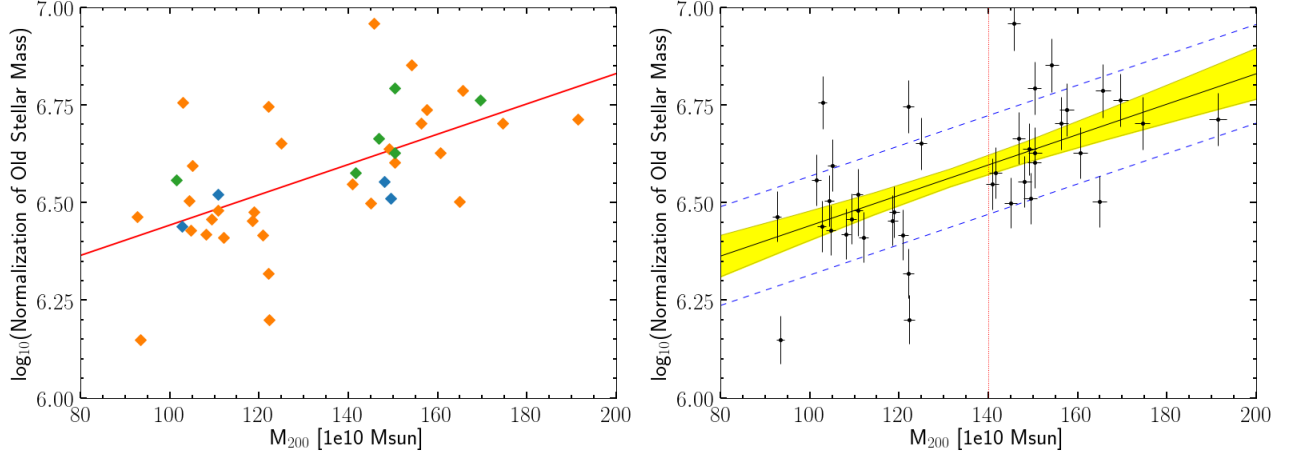

Fig. 5: *Left:* Scatter plot of $\log_{10}$(mass normalization) [i.e. b obtained above] against the virial mass $M_{200,c}$ of the Auriga haloes. We use linear regression to see whether there is a correlation, and find $a_2 = 0.00388$, $b_2 = 6.597$. Colours indicate resolution: L3 green, L4 orange, and L5 blue. *Right:* Same 'data', but MCMC fit. Red dotted line shows 'central' x value; yellow region 1σ interval; blue dashed lines intrinsic scatter. Fake Error bars (1% of the obtained values).
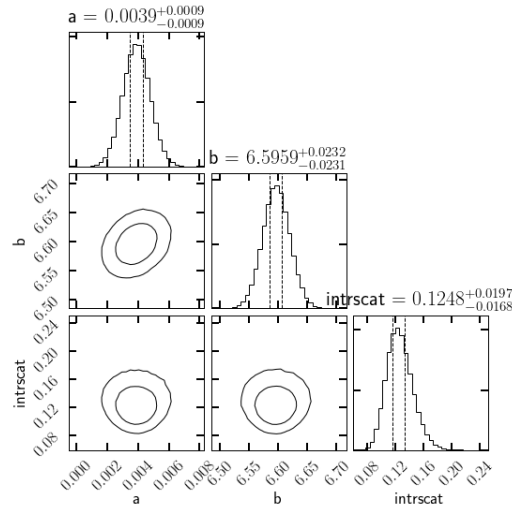
Fig. 6: TODO: corner plot of the MCMC. Conclusion: there is a positive correlation of the normalization of old stellar mass with the virial mass $M_{200,c}$.
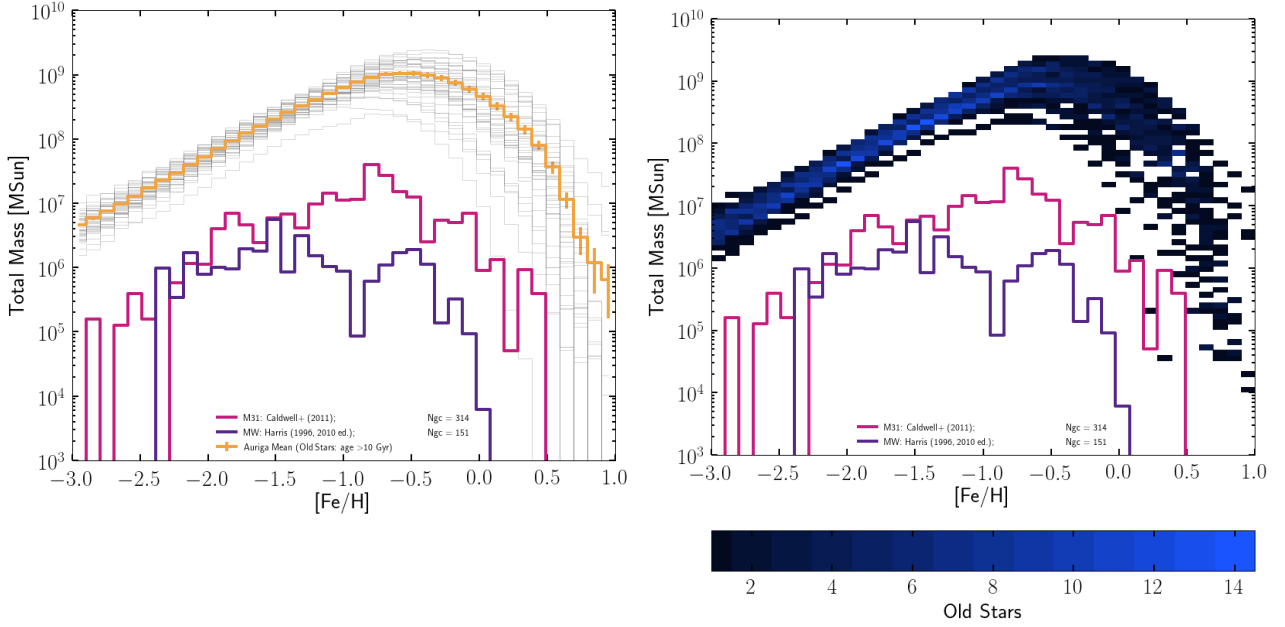
Fig. 7: *Left:* Mean value of all 40 simulations in orange. *Right:* Colorbar shows the number of simulations that fall in (arbitrary) bins in y-direction.
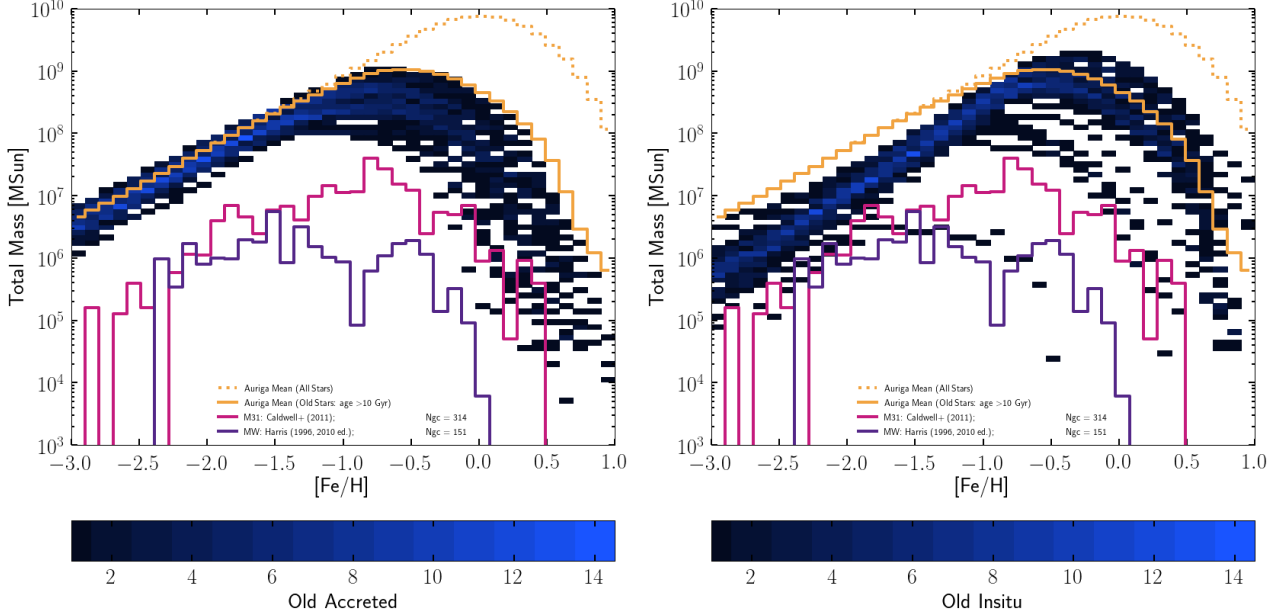

Fig. 8: *Left:* Mass-weighted [Fe/H] distribution of **Old accreted** (age > 10 Gyr) star particles. Solid orange line shows the mean of all old star particles in all Auriga simulation. The dotted orange line shows the mean of all star particles in all Auriga simulations (i.e. not enforcing an age cut). *Right:* Mass-weighted [Fe/H] distribution of **Old insitu** (age > 10 Gyr) star particles. *Both / Conclusion:* The metallicity range $-3 <$ [Fe/H] < -1 is only populated star particles older than ten Gyr; [Fe/H] > -1 is dominated by star particles younger than 10 Gyr (two orders of magnitude difference). Furthermore, the old accreted star particles contribute most significantly to the range $-3 <$ [Fe/H] < -1, and the contribution of the old insitu star particles at these metallicities declines steeper with declining metallicity than the old accreted population. The old insitu population provides the dominant contribution of the old population for [Fe/H] > -1.
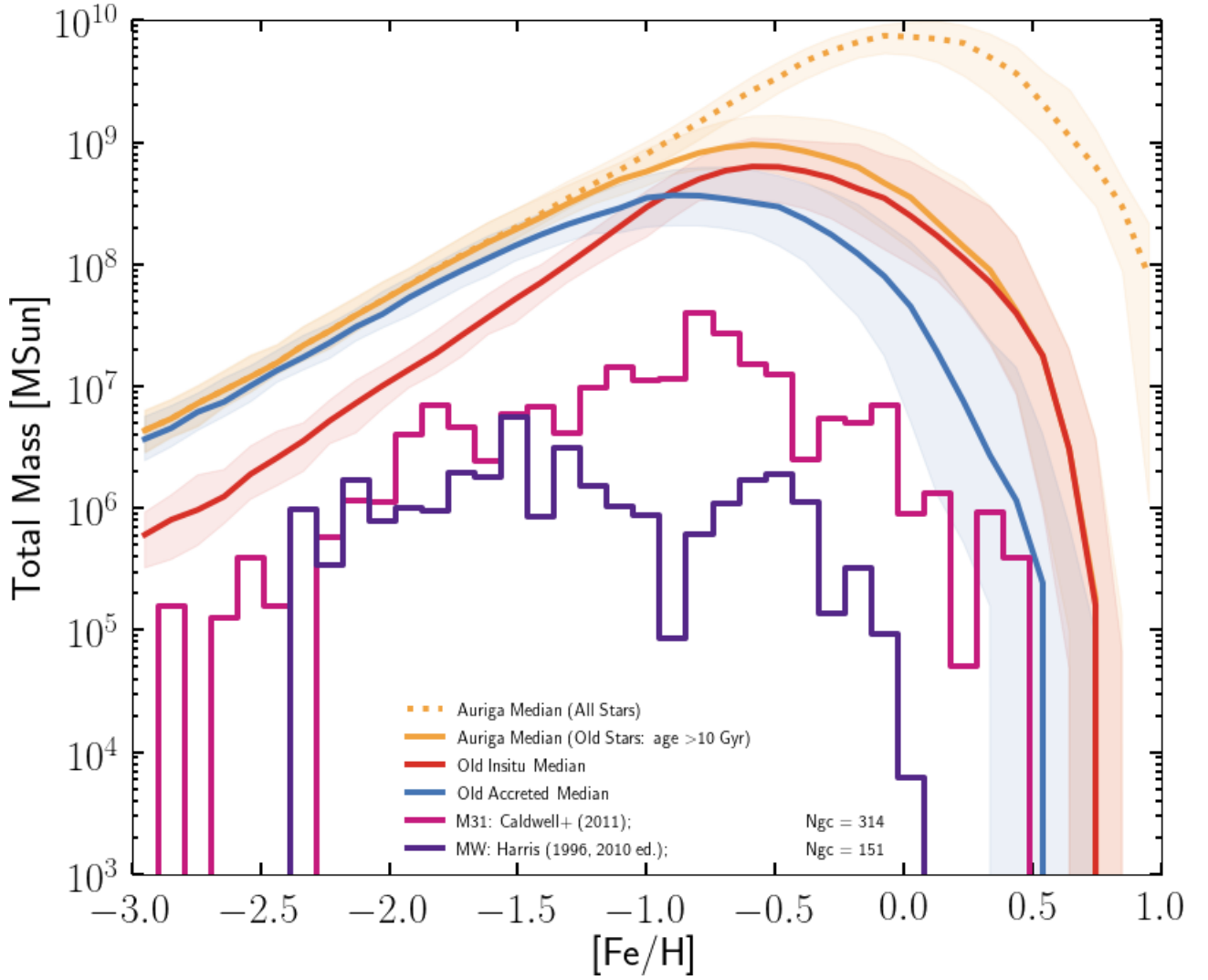
Fig. 9: Mass-weighted metallicity distribution of star particles in the Auriga simulations. We show the median value of all Auriga haloes for all stars (orange dotted) and globular cluster candidates (i.e. stars with age > 10 Gyr; orange solid). The latter sub set is further split up between stars that formed insitu (red solid), and those that were accreted (blue solid). Shaded regions indicate the 1σ interval. The MW GCS is shown in purple and that of M31 in pink. We use the same bin sizes for the simulations as for the observations, explicitly plotted for the observed profiles.
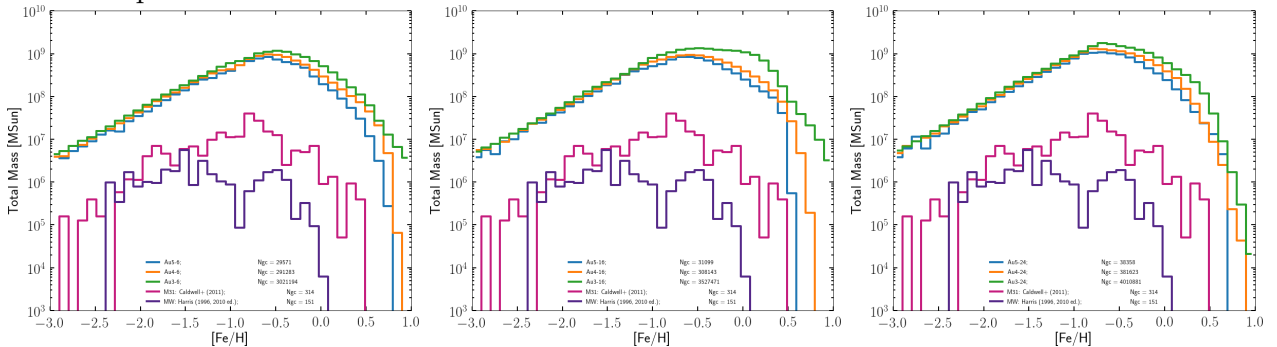
Fig. 10: Same figure, but now colours indicate resolution: L3 green, L4 orange, and L5 blue. *Left:* Auriga halo 6. *Mid:* Auriga halo 16. *Right:* Auriga halo 24. For all three haloes we find marginal increases in the mass normalization with increasing resolution level.

6

4.2   Distribution of Galactocentric radii r_gc
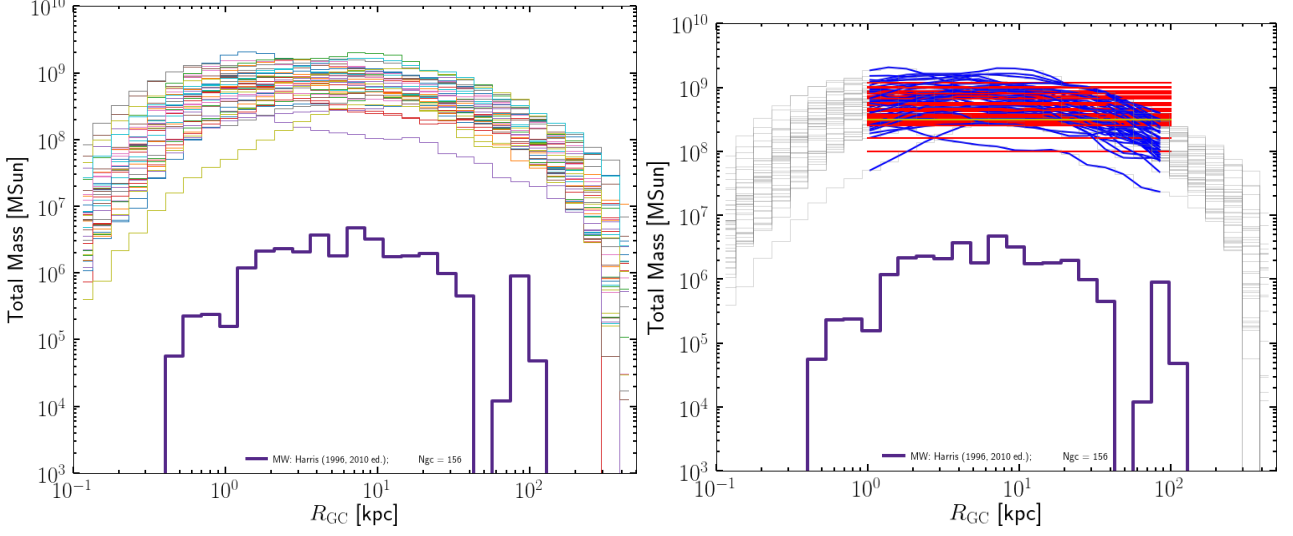
Fig. 11:   *Left:* Mass-weighted r_{gc} distribution of all Auriga haloes (level 3, 4 and 5). *Right:* We use linear regression to obtain $\log_{10}$(mass normalization) in the domain 0-100 kpc (i.e. we fit $ax + b$ with $a = 0$)
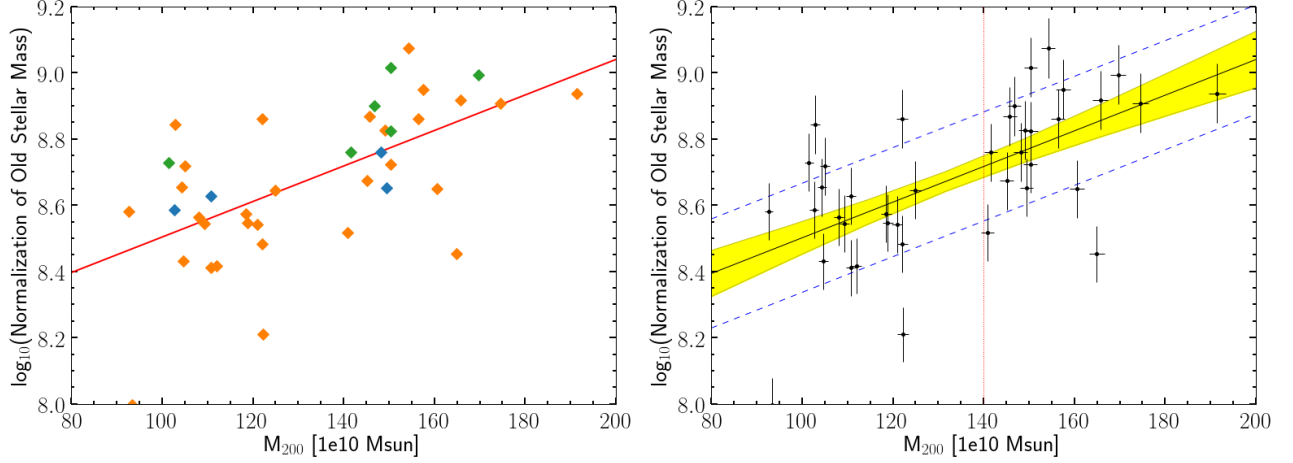

Fig. 12:   *Left:* Scatter plot of $\log_{10}$(mass normalization) [i.e. b obtained above] against the virial mass $M_{200,c}$ of the Auriga haloes. We use linear regression to see whether there is a correlation, and find $a_2 = 0.005$, $b_2 = 8.716$. Colours indicate resolution: L3 green, L4 orange, and L5 blue. *Right:* Same 'data', but MCMC fit. Red dotted line shows 'central' x value; yellow region 1σ interval; blue dashed lines intrinsic scatter. Fake Error bars (1% of the obtained values).
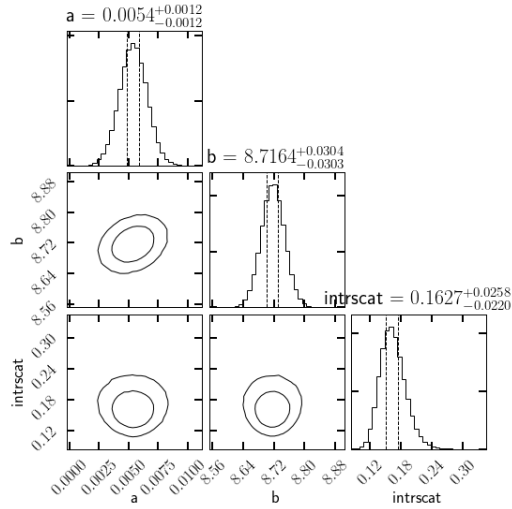
Fig. 13:   TODO: corner plot of the MCMC. Conclusion: there is a positive correlation of the normalization of old stellar mass with the virial mass $M_{200,c}$.
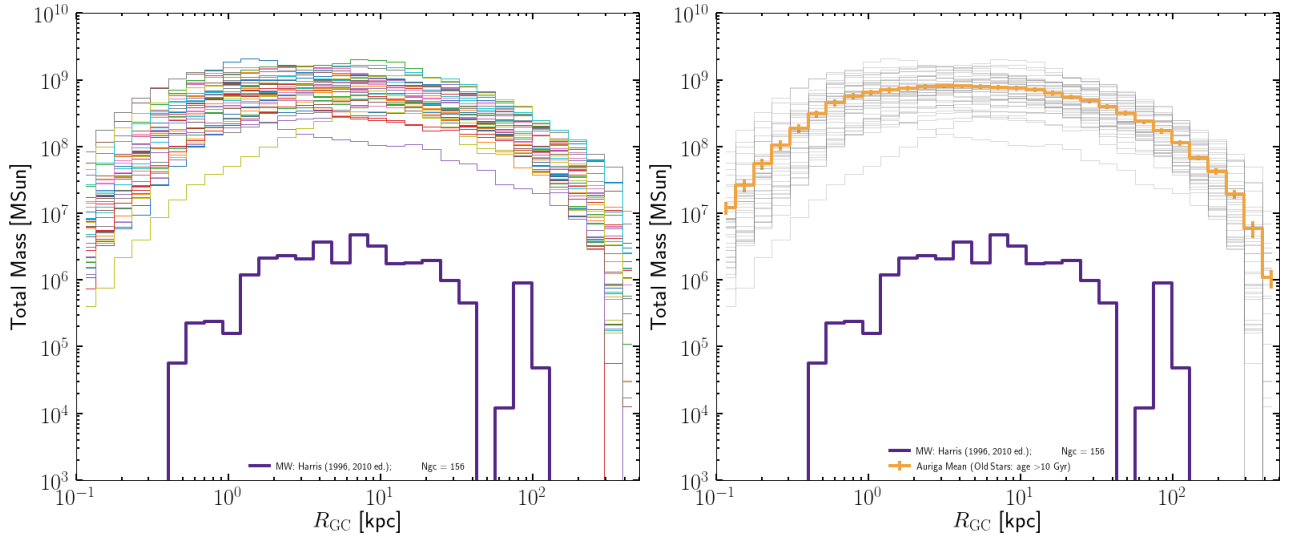
Fig. 14: *Left:* Mass-weighted r_{gc} distribution of all Auriga haloes (level 3, 4 and 5). *Right:*
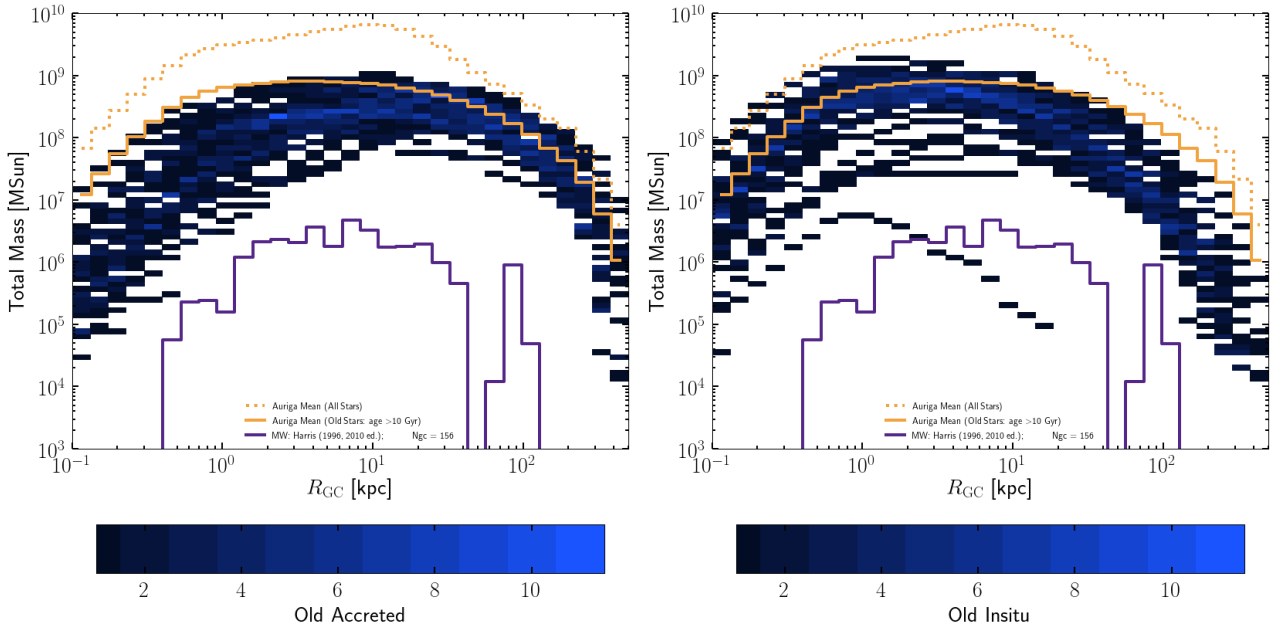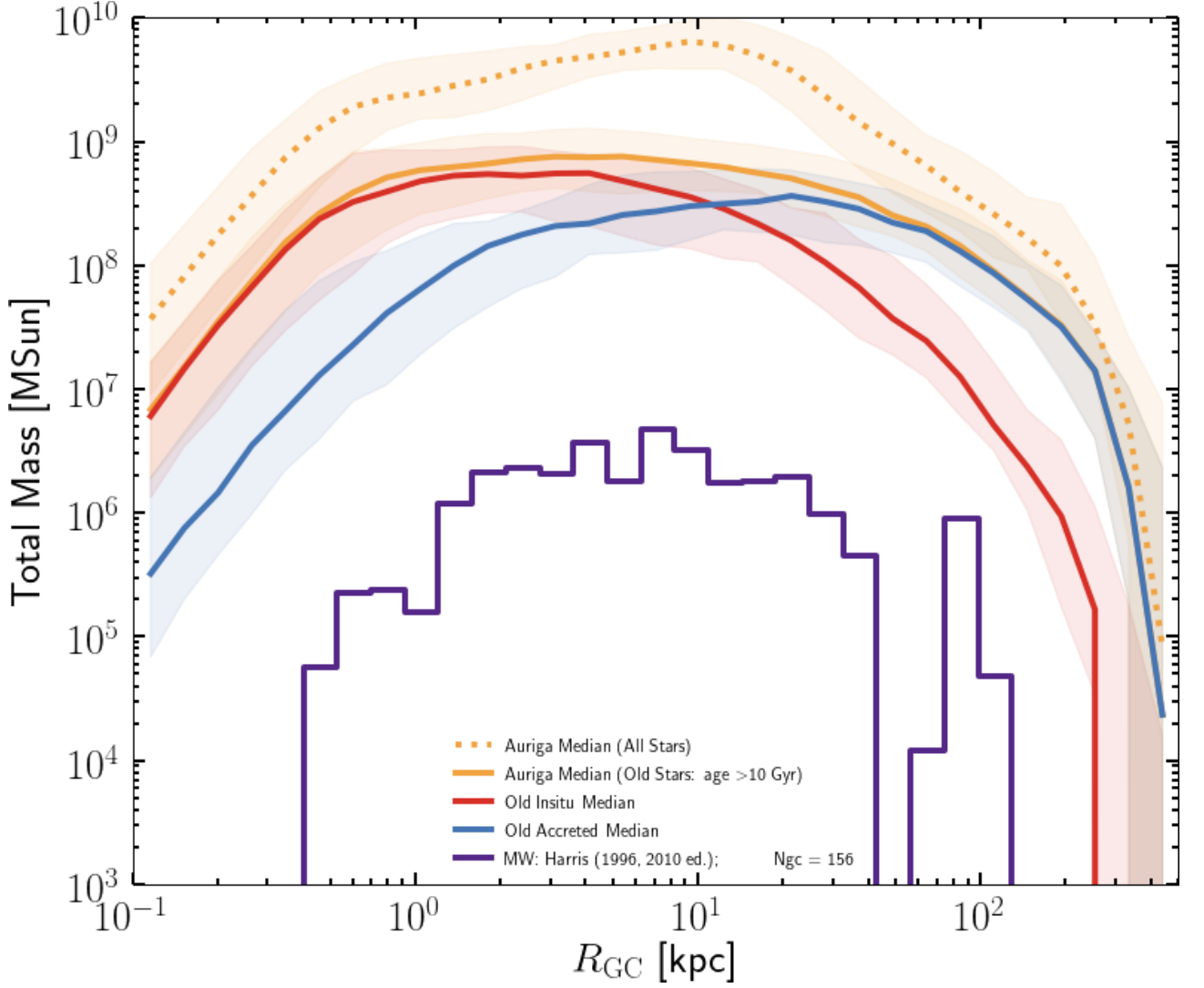

Fig. 15: *Left: Right:*

Fig. 16: Mass-weighted distribution of galactocentric radii at which star particles in the Auriga simulations are found. We show the median value of all Auriga haloes for all stars (orange dotted) and globular cluster candidates (i.e. stars with age > 10 Gyr; orange solid). The latter sub set is further split up between stars that formed insitu (red solid), and those that were accreted (blue solid). Shaded regions indicate the 1σ interval. The MW GCS is shown in purple and that of M31 in pink. We use the same bin sizes for the simulations as for the observations, explicitly plotted for the observed profiles.
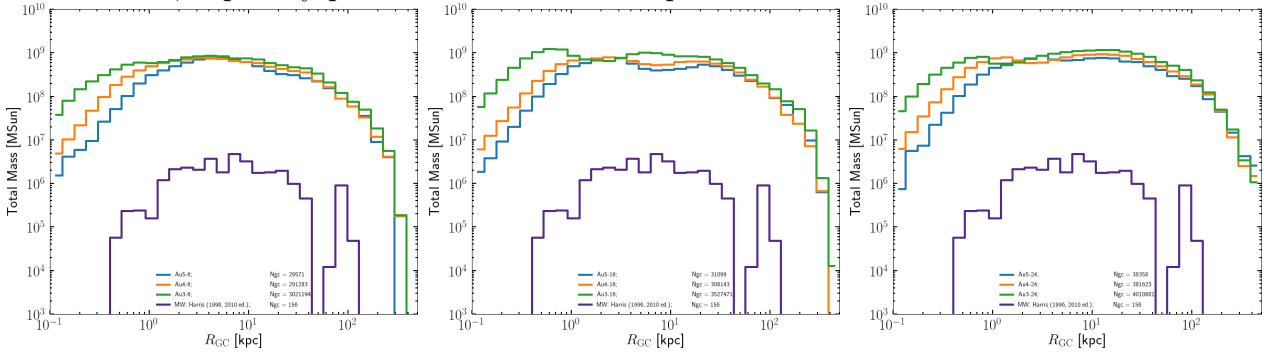
Fig. 17: Same figure, but now colours indicate resolution: L3 green, L4 orange, and L5 blue. *Left:* Auriga halo 6. *Mid:* Auriga halo 16. *Right:* Auriga halo 24. For all three haloes we find marginal increases in the mass normalization with increasing resolution level.
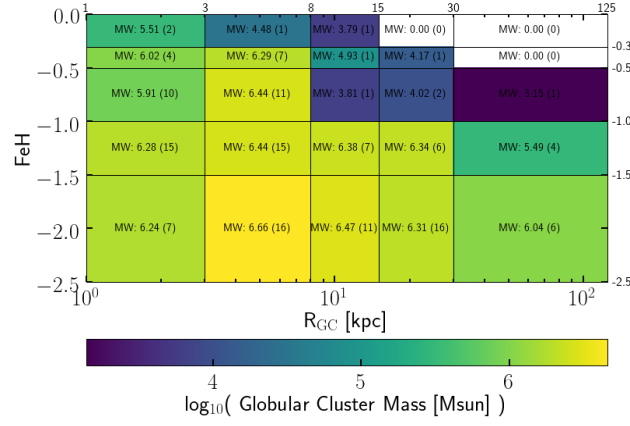
9

4.3   Distribution of [Fe/H]-r$_{gc}$

Fig. 18: Repetition of Fig. 2 (right) for (convenient) comparison. Note that the limits on the color bar are different for the observations and the mean of all simulations below.
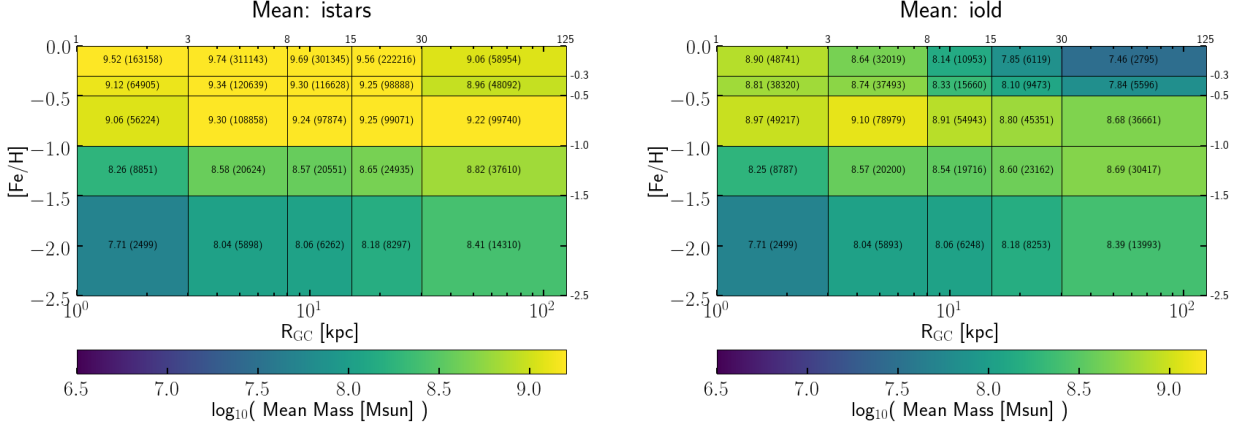

Fig. 19: *Left:* Mass-weighted [Fe/H]-r$_{gc}$ distribution of all Auriga haloes (level 3, 4 and 5). Here we consider all stars in all simulations and color-code the **mean value** (of 40 Auriga haloes) *Right:* Same figure, but for old (> 10 Gyr) stars.
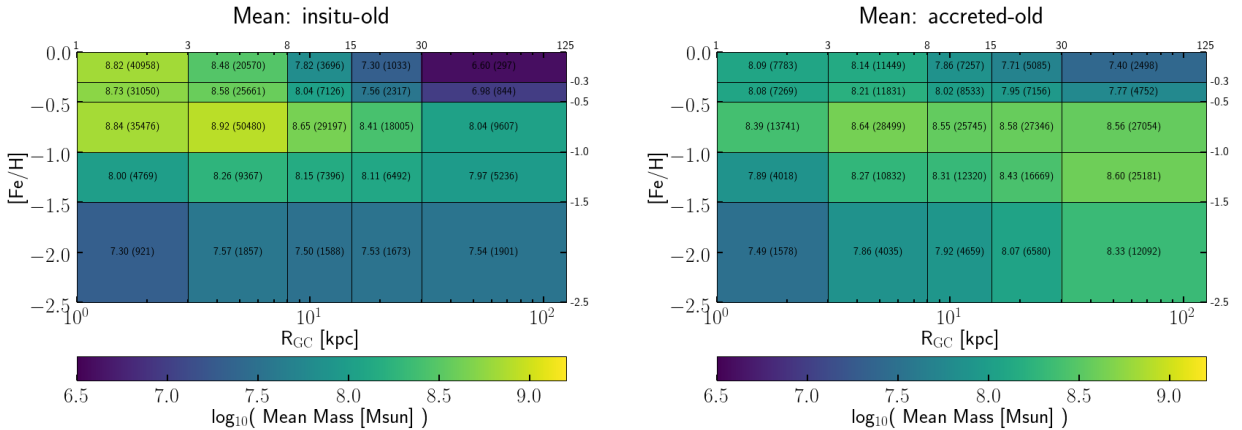

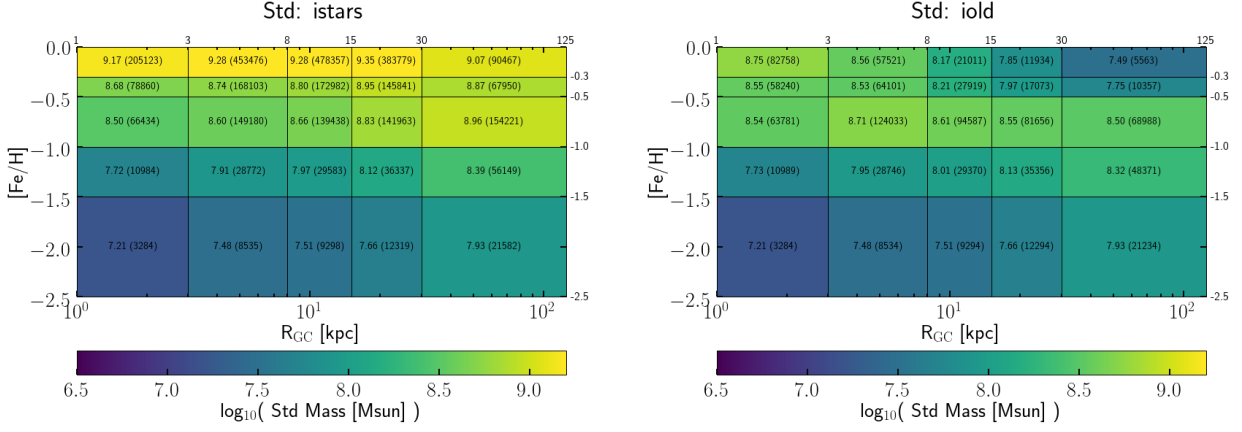Fig. 20: *Left:* Same figure, but for old insitu stars. *Right:* Same figure, but for old accreted stars.

Fig. 21: *Left:* Mass-weighted [Fe/H]-r$_{gc}$ distribution of all Auriga haloes (level 3, 4 and 5). Here we consider all stars in all simulations and color-code the **standard deviation** (of 40 Auriga haloes) *Right:* Same figure, but for old (> 10 Gyr) stars.
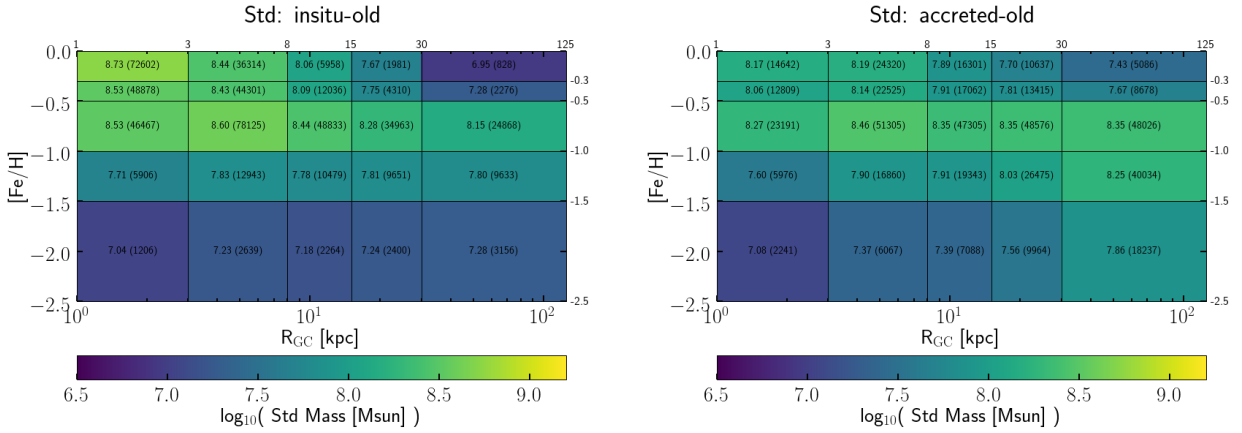

Fig. 22: *Left:* Same figure, but for old insitu stars. *Right:* Same figure, but for old accreted stars.
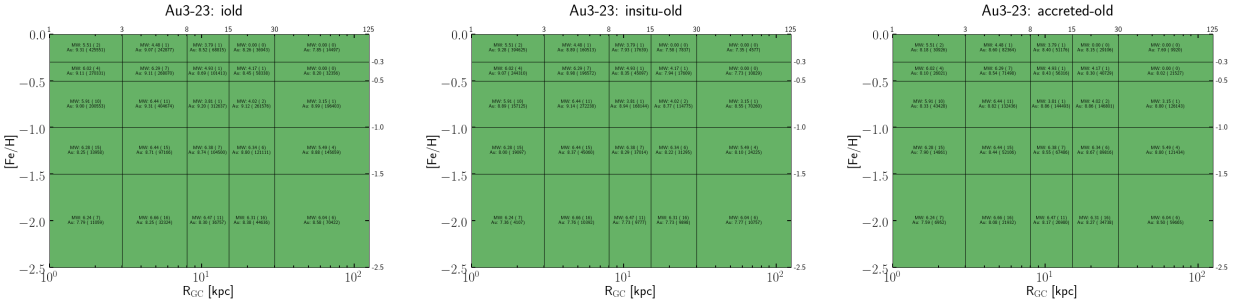

Fig. 23: Lazy comparison to check whether there is more (total) mass in the simulated star particles than in the MW GCS. Green means yes; red means no. We check this for all fourty haloes individually to answer the question whether the star formation model implemented in the Auriga simulations can produce 'stars in the right place'. *Left:* Au3-23, old stars. *Mid:* Au3-23: old insitu stars. *Right:* Au3-23: old accreted stars.

11

4.3.1 Distribution of [Fe/H]-r_{gc}: more bins / higher resolution
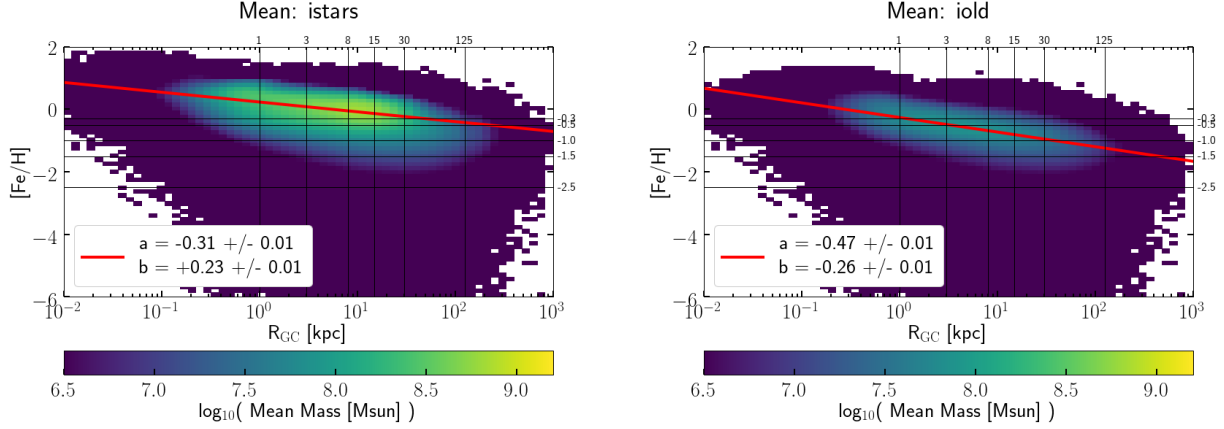

Fig. 24: *Left:* Mass-weighted [Fe/H]-r_{gc} distribution of all Auriga haloes (level 3, 4 and 5). Here we consider all stars in all simulations and color-code the **standard deviation** (of 40 Auriga haloes). Difference here is that we 'cranked up' the resolution, because we can and it's awesome. Note that the range is somewhat larger. Observational bin edges are indicated by horizontal and vertical lines for convenience. *Right:* Same figure, but for old (> 10 Gyr) stars. The red line shows a linear fit to the metallicity-radius relation, weighted by mass. The best-fit parameters are indicated in the lower left corner.
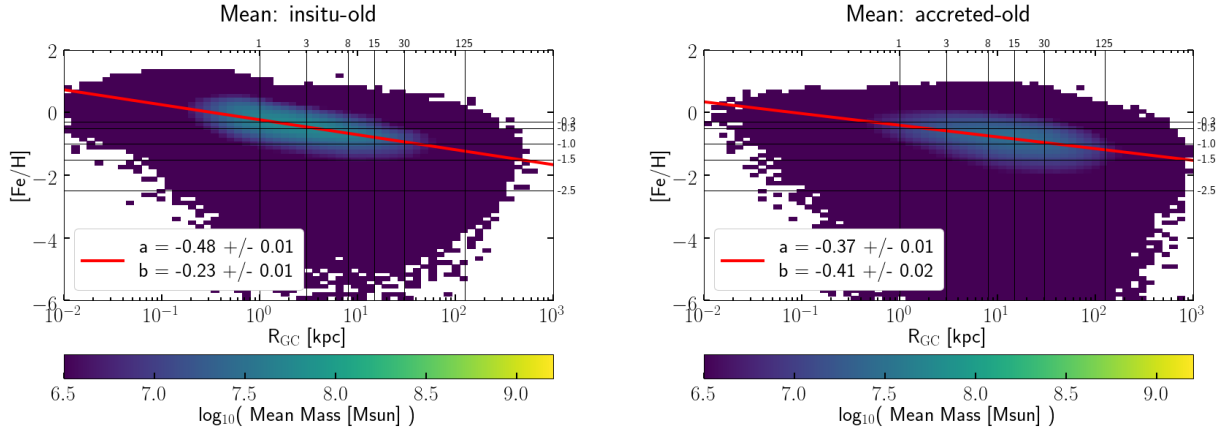

Fig. 25: *Left:* Same figure, but for old insitu stars. *Right:* Same figure, but for old accreted stars. Our linear fit shows the slope of the metallicity profile (a), as well as the zero crossing point at r_{gc}=1kpc. (b). We note that the b is 0.49 dex lower for old star particles than for all star particles. The radial profile of the old **accreted** star particles is 0.18 dex lower than that of the old **insitu** star particles. The gradient a of -0.48 and -0.37 is slightly higher than the findings of Harris 1998 Fig.8 p.235, who reports Δ[Fe/H] / Δlog R_{gc} = -0.30 for $R_{gc} \lesssim$ 10 kpc.
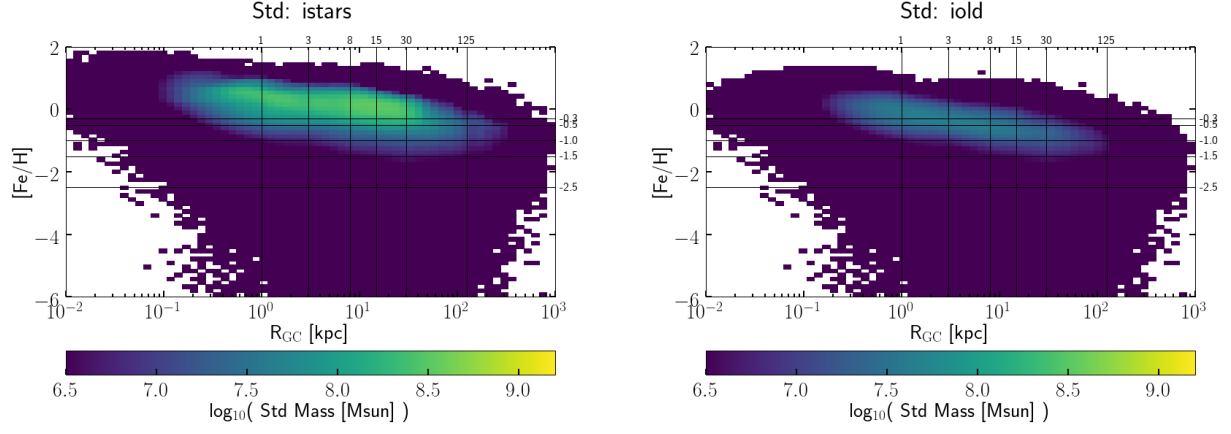
Fig. 26: *Left:* Mass-weighted [Fe/H]-r_{gc} distribution of all Auriga haloes (level 3, 4 and 5). Here we consider all stars in all simulations and color-code the **standard deviation** (of 40 Auriga haloes). *Right:* Same figure, but for old (> 10 Gyr) stars.
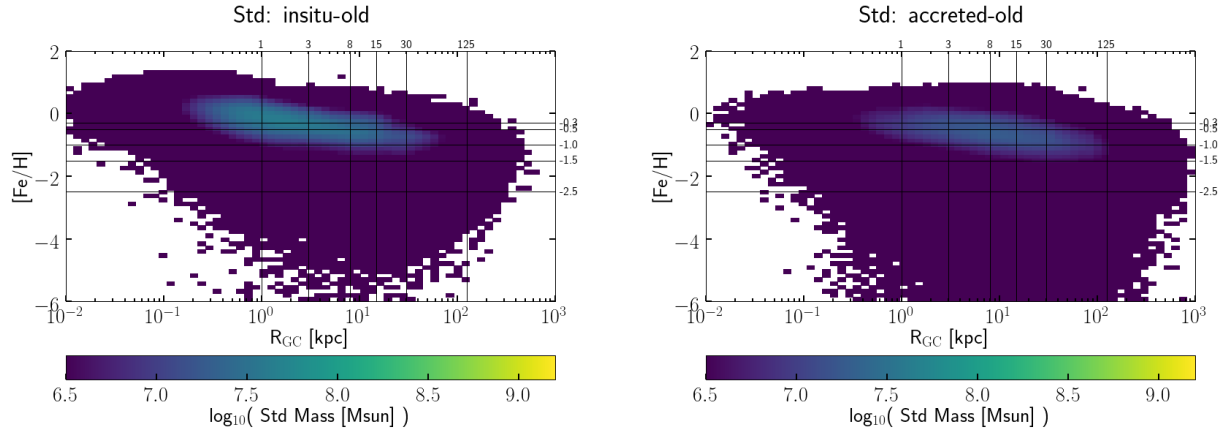

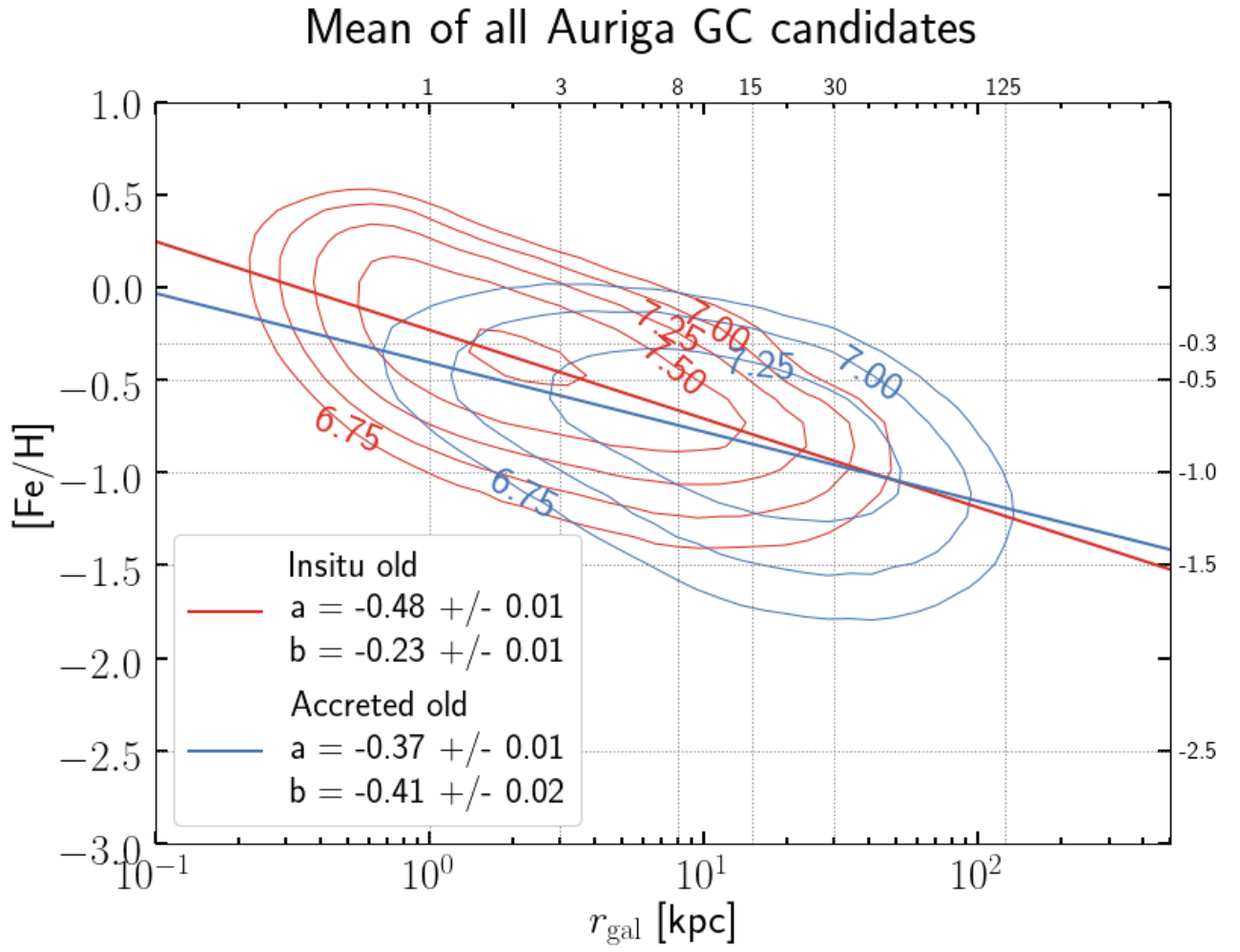Fig. 27: *Left:* Same figure, but for old insitu stars. *Right:* Same figure, but for old accreted stars.

Fig. 28: OMG what a beautiful plot.

4.4 Properties of birth haloes of the accreted population

A   MCMC

Bayesian code as described in and distributed by Andreon & Bergé (2012) and used in Andreon & Congdon (2014) for analysing the determination of the evolution of the richness-mass scaling. Code used is JAGS (Plummer et al., 2003), and the Python wrapper PYJAGS, and for laziness CORNER (Foreman-Mackey, 2016) for visual inspection.

Text could be something like the following. Blabla "we adopt this Bayesian approach.", and blabla "We assume weak priors on slope, intercept, and intrinsic scatter and solve for all variables at once. We used a computationally inexpensive 10 thousand long Markov chain Monte Carlo, discarding the initial 3 thousand elements used for burn-in. By running multiple chains, we checked that convergence is already achieved with short chains."

References

Andreon S., Bergé J., 2012, A&A, 547, A117

Andreon S., Congdon P., 2014, A&A, 568, A23

Caldwell N., Schiavon R., Morrison H., Rose J. A., Harding P., 2011, AJ, 141, 61

Foreman-Mackey D., 2016, The Journal of Open Source Software, 24

Harris W. E., 1996, AJ, 112, 1487

Pfeffer J., Kruijssen J. M. D., Crain R. A., Bastian N., 2018, MNRAS, 475, 4309

Plummer M., et al., 2003, in Proceedings of the 3rd international workshop on distributed statistical computing.

Renaud F., Agertz O., Gieles M., 2017, MNRAS, 465, 3622

VandenBerg D. A., Brogaard K., Leaman R., Casagrande L., 2013, ApJ, 775, 134